Simultaneous profiling of DNA methylation and chromatin architecture in mixed populations and in single cells

Guoqiang Li[1,6], Yaping Liu[3,4,6], Yanxiao Zhang[1], Rongxin Fang[1,5], Manolis Kellis[3,4], Bing Ren[1,2]*

[1] Ludwig Institute for Cancer Research, La Jolla, CA 92093

[2] Department of Cellular and Molecular Medicine, Center for Epigenomics, Institute of Genomic Medicine, Moores Cancer Center, University of California, San Diego, School of Medicine, La Jolla, CA 92093

[3] Broad Institute of MIT and Harvard, Cambridge, MA 02142

[4] Massachusetts Institute of Technology, Computer Science and Artificial Intelligence Laboratory, Cambridge, MA 02139

[5] Bioinformatics and Systems Biology Graduate Program, University of California, San Diego, La Jolla, CA 92093

[6] Contributed equally

* email: biren@ucsd.edu

Abstract

Dynamic DNA methylation and three-dimensional chromatin architecture compose a major portion of a cell's epigenome and play an essential role in tissue specific gene expression programs. Currently, DNA methylation and chromatin organization are generally profiled in separate assays. Here, we report Methyl-HiC, a method combining *in situ* Hi-C and whole genome bisulfite sequencing (WGBS) to simultaneously capture chromosome conformation and DNA methylome in a single assay. Methyl-HiC analysis of mouse embryonic stem cells reveals coordinated DNA methylation between distant yet spatially proximal genomic regions. Extension of Methyl-HiC to single cells further enables delineation of the heterogeneity of both chromosomal conformation and DNA methylation in a mixed cell population, and uncovers increased dynamics of chromatin contacts and decreased stochasticity in DNA methylation in genomic regions that replicate early during cell cycle.

Main

DNA methylation plays a critical role in gene regulation[1]. DNA methylation is dynamically regulated by a variety of enzymes, including the *do novo* methyltransferases DNMT3a and DNMT3b and the ten-eleven translocation (TET) family of dioxygenases TET1/2/3[2]. Additionally, DNA methylation patterns are maintained by DNMT1[3]. The methylation status of adjacent CpG dinucleotides on the same DNA fragment is often coordinated, a phenomenon that has been used to define methylation haplotype in liquid biopsy tests[4,5]. However, due to the short fragment length in Whole Genome Bisulfite Sequencing (WGBS)[6] and absence of long-read methylome sequencing technologies[7,8], it is not clear how long such coordinated DNA methylation extends in mammalian cells. As the DNA is spatially organized into three-dimensional structures, genomic regions that reside up to hundreds of kilobases away can be brought into spatial proximity through chromatin folding[9]. Thus, it is conceivable that DNA methylation between distal sequences could also be coordinated due to their spatial proximity. The chromosome conformation capture (3C) technology is based on proximal ligation of spatially close genomic DNA segments[10,11]. Since DNA methylation is a covalent modification on DNA, methylation status of cytosines far apart on the linear sequence could in principle be captured simultaneously on ligated DNA during chromosome conformation capture procedures. We exploit this principle to develop Methyl-HiC, combining *in situ* Hi-C[12] and WGBS to simultaneously profile chromatin organization and DNA methylation genome-wide (Fig. 1a). Briefly, long-range chromatin interactions are captured by crosslinking with formaldehyde, digested with methylation insensitive restriction enzyme DpnII, labeled with biotinylated nucleotides, and ligated *in situ*. The ligation products are then enriched with streptavidin coated magnetic beads after sonication of genomic DNA. The captured DNA is then subject to bisulfite conversion, library construction and paired-end sequencing (Fig. 1a). We developed a computational pipeline, Bhmem, to map the sequencing reads to the reference genome, reveal the methylation status on linked DNA fragments (Fig. 1b and Supplementary Fig. 1a) (see Method for description of Bhmem) and compute the pairwise contact frequency genome wide.

To demonstrate the performance of Methyl-HiC, we first applied it to the mouse embryonic stem cell line F123, a hybrid between the castaneus and S129/SvJae mouse strains. We compared the results with that from *in situ* Hi-C analysis from the same cell line. With similar sequencing depth, Methyl-HiC results are highly correlated with *in situ* Hi-C at different resolutions (Fig. 1c, stratum-adjusted correlation coefficient (SCC)[13] in 250kb resolution: 0.92±0.02; SCC in 25kb resolution: 0.88±0.008). The contact probabilities of two datasets are comparable to each other (Fig. 1d). The chromatin loops, detected using HiCCUPS[12] at different resolutions, largely overlap between the two datasets (Fig. 1c, blue squares, and Supplementary Table 1). Additionally, chromatin loops identified from Methyl-HiC results showed similar enrichment of enhancers and promoters as marked by histone markers (H3K4me1, H3K27Ac, and H3K4me3), CTCF, and Polycomb-Repressed chromatin (H3k27me3), as *in situ* Hi-C, indicating that Methyl-HiC can effectively detect chromatin loops (Supplementary Fig. 1b). Furthermore, the Topologically Associating Domains (TADs) identified from the two datasets are also similar (Fig. 1e and Supplementary Fig. 1c). These results show that Methyl-HiC can capture chromosomal conformation as effectively as *in situ* Hi-C.

In addition to efficiently capturing chromosomal architecture, Methyl-HiC also profiles DNA methylation genome wide. We compared Methyl-HiC data with WGBS data from the same cell line and found that Methyl-HiC can capture about 80% CpGs from WGBS data (Fig. 1f). The methylation level of these CpGs showed great concordance (R=0.87, p<2.2-e16) with WGBS results (Fig. 1g and Supplementary Fig. 1d). We also notice that Methyl-HiC reads tend to be enriched at regions with DNA hypomethylation. Despite this bias, Methyl-HiC accurately measures the DNA methylation state for the over 15 million CpGs in the mouse genome (Fig.1g). These results, taken together, demonstrate that Methyl-HiC can simultaneously map DNA methylome and chromatin architectures in a biological sample.

Previous studies have reported that adjacent CpGs usually share concordant methylation status, and the stretches of DNA that contain such CpGs are termed methylation haplotype blocks[4,5]. Because the genome is not only linearly separated but also spatially organized, we hypothesize that spatially proximal DNA may also have coordinated methylation status. To test this hypothesis, we analyzed the chromatin loops detected from

Methyl-HiC and *in situ* Hi-C in the same cell type. Indeed, the Pearson correlation coefficients of the methylation status from Methyl-HiC read pairs mapped to anchors of these chromatin loops (Supplementary Fig. 2a) are significantly higher than that from shuffled read pairs mapped to the same anchor regions (Fig. 2a and Supplementary Fig. 2b) (p<2.2e-16, Fisher z-transformation), indicating that methylation status of spatially proximal CpGs is coordinated. We further classified the loops according to the chromatin compartments they belong to. We observed that loop anchors in compartment A had higher methylation concordance compared to these in compartment B (Fig. 2b). This is in line with recent reports that the methylation correlation signal is a better predictor of A/B compartments than the average methylation signal[14].

Active and poised enhancers frequently exhibit hypomethylation in cells, and it is not clear whether the variable DNA methylation at enhancers is correlated with target gene promoters or other enhancers in the same transcription hub. Methyl-HiC data provides an opportunity to address this question. We classified the F123 cell genome into 7 different chromatin states using ChromHMM analysis of four histone modifications (H3K4me3, H3K4me1, H3K36me3, and H3K27me3)[15]. Pearson correlation coefficients of DNA methylation on the same Methyl-HiC read pairs showed different trends for pairs of genomic regions from different chromatin states. Methylation of DNA at actively transcribed genes, which are generally marked by H3K36me3, shows negative correlation with methylation status of active promoters and enhancers (Fig. 2c), consistent with previous observation that DNA methylation on TSS and gene body are inversely correlated[16]. By contrast, DNA methylation from active enhancer-like regions, marked by H34K4me1/3, shows positive correlation with that of linked promoters marked by H3K4me3, supporting the coordinated DNA methylation processes between active enhancers and their target gene promoters. Surprisingly, DNA methylation levels at regions with active enhancer-like chromatin state also display a positive correlation with that at linked regions marked by Polycomb-repressed chromatin state (Fig. 2c). This finding raises interesting questions regarding the relationships among polycomb-repressed state and enhancers, which will require additional experiments to resolve in the future.

Methods to map DNA methylome in single cells have been developed[17-19], and used to deconvolute sub-populations from heterogeneous tissues or cell populations. Similarly, approaches to map chromatin organization in single cells have also been devised to reveal cell to cell variations in chromosome conformation in a mixed cell population[20-22], and to study chromatin architecture in cell cycle[23] and rare cell types, such as oocytes and zygotes[24]. One drawback of these methods is that DNA materials are destroyed during the process, preventing analysis of different epigenomic features from the same cells. The development of Methyl-HiC would overcome this limitation and provide the opportunity to explore the heterogeneity of DNA methylation and chromatin architecture simultaneously in a mixed cell population. We therefore modified methyl-HiC protocols to single cells. Briefly, after *in situ* proximal ligation, we sort individual nuclei into a 96-well plate, and then perform bisulfite conversion in each well. DNA adaptors are next ligated to the resulting bisulfite-converted single strand DNA (ssDNA), and the resulting DNA is PCR amplified for paired-end sequencing[17] (Fig. 3a). We generated single cell Methyl-HiC data for 108 mES cells cultured in serum plus LIF condition (primed state) and 48 mESCs cultured in 2i conditions (naïve state)[25]. After removing low quality reads (mapQ<30), PCR duplicates, and inter-chromosomal read pairs, and cells with less than 250,000 reads and 10,000 *cis* ligations, we obtained data for 103 primed state mESCs and 47 naïve mESCs, each with about 1 million uniquely mapped and high quality intra-chromosomal reads for further analysis (Supplementary Table 2). Reads with each end originating from distinct restriction fragments are selected for further analysis, resulting in around 100,000 contacts on average in each cell (Supplementary Fig. 3a). The contact probabilities are comparable between the bulk dataset and the aggregate of single cells (Supplementary Fig. 3b). After normalization for sequencing coverage[26], the intra-chromosomal interaction matrix from the bulk dataset and ensemble dataset of 103 primed mESCs are very comparable (Fig. 3b and Supplementary Fig. 3d, 3e), with the Pearson correlation coefficient computed from observed over expected contact matrix (250kb bin resolution) at 0.98 (p<2.2e-16). We also generated single cell methylomes from these cells with an average coverage of 288,000 CpGs per cell, a level that is comparable to previous single cell Methylome datasets[17,18] (Supplementary Fig. 3c). The average methylation levels of primed and naïve mESCs are around 60% and 20% (Fig. 3c), respectively, consistent with previous single cell DNA methylome data[18]. Moreover, consistent with the observation from bulk

populations, DNA methylation levels at the loop anchors are coordinated in individual cells (Fig. 3d). Taken together, these results show that our single cell Methyl-HiC can capture DNA methylation and chromatin architecture simultaneously in single cells.

The single cell Methyl-HiC dataset would enable analysis of cell-to-cell variability in both chromosome organization and DNA methylation as they relate to different replication timing regions. DNA replication is accompanied by dynamic chromosome organization and DNA methylation. In particular, previous studies have uncovered a link between chromatin compartments and timing of DNA replications, and between topologically associating domains with DNA replication domains[27,28]. While DNA methylation pattern is generally replicated by the DNMT1 at each cell division, the fidelity is not 100%, resulting in variation and plasticity in the methylome[29]. We partitioned the genome into four groups based on replication timing previously determined by Repli-ChIP data from mESC[30]. We then analyzed single cell methylomes and 3D interactions in each replication timing group. We found that regions associated with late replication showed higher DNA methylation levels (Supplementary Fig. 3f), consistent with their heterochromatin nature[31]. Moreover, the late replication regions tend to show higher cell-to-cell variability of DNA methylation evidenced by increased Standard Deviation (SD) across 107 mESCs (Fig. 3e) and a higher rate of hemi-methylation (CpGs with methylation level equal to 0.5 in single cell DNA methylome) (Supplementary Fig. 3g). Interestingly, late-replicating DNA had lower variabilities in chromatin interactions than early-replicating DNA (Fig. 3f). Taken together, our data suggest that early replication regions are characterized by more dynamic long-range interactions, less variable DNA methylation, more permissive chromatin states and higher gene expression level[32], than late replication time domains.

Epigenetic heterogeneity in tissues or cell population presents a significant challenge in analysis of epigenome of tissue samples[17,33]. As DNA methylation differs among different cell types, it is possible to deconvolute distinct cell types from single cell Methyl-HiC datasets based on DNA methylation so that the chromatin contacts could be investigated in each cell type. Indeed, the primed and naïve mESCs were clearly separable using single cell Methyl-HiC datasets (Fig. 4a). Interestingly, the primed mESCs can be further divided into two subpopulations according to DNA methylome, which is consistent with previous

report[18] (Fig. 4a). We then compared these subpopulations with lineage specific DNA methylation profiles from ENCODE projects and found that the two subpopulations in primed cells clustered with different lineages specific features, in which Cluster 3 showed potential embryonic limb development trend (Fig. 4b). We then aggregated the contact matrix of cells that share the same DNA methylation status, and compared the populations to each other as well as clearly defined mESCs cells. Our result showed that the aggregated contact matrix could show heterogeneity between different DNA methylation clustered cells (Fig. 4c), which suggests that our method will be useful to determine single cell HiC identity of heterogeneous cell population and tissues. To further show the biological function of the 3D structure heterogeneity, we identified the differential compartments between two clusters (Supplementary Table 3). Genome ontology (GO) analysis of the Differential Methylated Regions (DMRs) and genes located in these differential compartments revealed that DMRs and genes that switched from compartment B in Cluster 2 to compartment A in Cluster 3 were enriched for genes with function related to embryonic limb development (Fig. 4d and 4e). For example, *HoxD* cluster genes and *Epha4* are key regulators for embryonic limb development[34,35]. Here we showed that *HoxD* cluster genes and *Epha4* gene switched from compartment B in Cluster 2 to compartment A in Cluster 3 (Fig. 4f and Supplementary Fig. 4). This is in line with our above clustering according to DNA methylome, indicating that our method can discover differential chromatin conformations in heterogeneous cells.

Here, we report a novel method, Methyl-HiC, which combines high throughput chromatin conformation capture with whole genome bisulfite sequencing that can simultaneously profile and integrate two epigenetic regulations on the same DNA molecule. We demonstrate that Methyl-HiC could be used to study the higher-order organization of chromosomal structures and DNA methylomes simultaneously in mixed populations and in single cells. By doing these, we show that DNA methylation status is generally concordant between spatially close cytosines.

The simultaneous profiling of multiple epigenomic features, especially from single cells, has multiple advantages over assaying each feature individually. As the cost of both Hi-C and WGBS is predominantly sequencing, combining two assays together will lead to

substantial savings due to reduced sequencing cost. In addition, Methyl-HiC is desirable when the biological material is limited, such as oocytes, zygotes and early embryos. In particular, single cell Methyl-HiC generates maps of DNA methylome and chromosome conformation from the same cells, allowing integrative analysis of chromatin architecture and epigenome in individual cells. While current protocol of single cell Methyl-HiC is still limited by data sparsity, this limitation could be overcome in the future by better DNA methylation detection strategies, such as bisulfite free DNA methylation profiling[36], or better amplification approaches, such as META (multiplex end-tagging amplification)[37]. Further development of single cell Methyl-HiC in the future to include variants detection from bisulfite reads[38] and transcriptome[39,40] from the same cell will allow us to reveal the comprehensive regulation diagram in a single cell from genetic, epigenetic, transcription, and chromatin interaction aspects.

Although single cell epigenomic datasets can be clustered *de novo*, the identities of each sub-population are difficult to determine because of the stochasticity of epigenomic regulation and lack of reference epigenome from previously characterized cell types, especially for assays like single cell Hi-C that the reference of rare populations are very hard to profile. DNA methylation is a stable and cell-type specific epigenetic modification, which has proved to be capable for analyzing the cell composition of heterogeneous samples, such as neuronal subtypes in cortex[17]. Thus, by combining single cell DNA methylation with single cell Hi-C, chromosome conformation heterogeneity can be revealed by grouping via DNA methylation. Because of its low cell-input requirements, single cell Methyl-HiC is readily applicable to diverse samples, tissue types, and rare cell populations, which will benefit our understanding of the chromosome conformation in different conditions.

Methods

Cell culture

The F1 Mus musculus castaneus × S129/SvJae mouse ESC line (F123) was a gift from the laboratory of E. Heard and has been described previously[41]. Cells in primed state were cultured with irradiated mouse embryonic fibroblasts (Gibco, A34180) in medium with 85% DMEM, 15% Knock-out Serum Replacement (Gibco, 10828-028), 1X penicillin/streptomycin, 1X non-essential amino acids (Gibco, 11140-050), 1X GlutaMax (Gibco, 35050), 0.4 mM β-mercaptoethanol and 1000U/ml LIF (Millipore, ESG1107). Cells in naïve state were adapted from primed cells by passaging cells in MEF free and serum free conditions in 2i medium, which contained 50% NEUROBASAL (Gibco 21103-049), 50% DMEM/F12 (Gibco 11320-033), 0.5% N2-SUPPLEMENT (Gibco 17502-048), 1% B27+RA (Gibco 17504-044), 0.05% BSA (Gibco 15260-037), 1X penicillin/streptomycin, 2mM GLUTAMINE (Gibco 25030-081), 150 μ M Monothioglycerol (Sigma M6145), 1000U/ml LIF (Millipore, ESG1107), 1 μ M MEK inhibitor (Stemgent 04-0006), and 3 μ M GSK3 inhibitor (Stemgent 04-0004). Primed cells were collected and plated on 0.2% gelatin-coated feeder-free plates for 30 mins before harvesting to remove feeder cell contamination.

Methyl-HiC

In situ Hi-C was performed according to previous protocol[12]. Briefly, two million cells were cross-linked with 1% formaldehyde for 10 min at room temperature. Reaction was then quenched with 0.2M Glycine. Cell pellets were washed with cold PBS and lysed with lysis buffer to get nuclei pellets. Nucleus were permeabilized with 0.5% SDS. DNA was *in situ* digested with 100 units of DpnII (NEB) overnight. The ends of restriction fragments were filled with biotinylated nucleotides and *in situ* ligated. After reversal of crosslinks, ligated DNA was ethanol precipitate and sheared to a length of ~400bp by sonication (Covaris). Sonicated products were pulled down with streptavidin beads. Library construction was then performed on beads. After adapter ligation, beads were suspended in 20ul TE buffer and subjected to bisulfite conversion with EZ DNA Methylation-Gold™ Kit (Zymo, D5005).

Unmethylated lambda DNA was sonicated and ligated with the same adapter for Methyl-HiC sample and then was spiked in at 0.5% before bisulfite conversion. After conversion, streptavidin beads were removed with magnet and the supernatant were purified. Purified bisulfite converted DNA was amplified with HiFi Hotstart Uracil+Ready Mix (KAPA, KK2802).

Single cell Methyl-HiC (scMethyl-HiC)

In situ Hi-C was performed as same as above bulk Methyl-HiC till proximal ligation. After ligation, nuclei pellets were centrifuged and washed with PBS. Pellets were suspended in PBS stained with 1:200 DRAQ7 (CST, 7406S). FACS sorted single nuclei were directly added to 96 well plate with 9ul PBS in each well. Sorted nuclei were then briefly centrifuged and bisulfite conversion was directly performed on the sorted nuclei with EZ-96 DNA Methylation-Direct™ Kit according to the manufactory manual (Zymo, D5020). 0.5% of fragmented lambda DNA was spiked in before bisulfite conversion. Following bisulfite conversion of single nuclei, random priming of bisulfite-converted DNA with high concentration Klenow fragments (Enzymatics, P706L) incorporates an indexed P5 adapter to 5' ends of synthesized fragments, which can be used for downstream multiplexing capability. Exonuclease I and Shrimp Alkaline Phosphatase (NEB) treatments were then performed to digest unused random primer and inactivate dNTPs, followed by a SPRI bead-based purification step. P7 adapter were then ligated to the 3' end of single-stranded products by Adaptase module (Swift, 33096)[42]. Library amplification was then performed using indexed primers that incorporate dual indexing to enable 96-plex sequencing. Amplified libraries were pooled together and subjected to size selection and library quantification.

Whole-genome bisulfite sequencing

Genomic DNA was first extracted from mESCs (DNeasy Blood & Tissue Kit, Qiagen). 1–1.5 μg of genomic DNA was fragmented by sonication (Covaris), end-repaired, dA-tailed and ligated to cytosine methylated Illumina Truseq adapter. Ligation product was

subjected to bisulfite conversion reaction according to the manufacturer's instructions (EZ DNA Methylation-Gold Kit, Zymo, D5005). 0.5% unmethylated λDNA was spiked-in before the conversion. Bisulfite converted DNA was then PCR amplified and purified.

Sequencing of DNA libraries

The quantification of sequencing libraries was determined by qPCR and TapeStation DNA analyzer (Agilent Technologies). Pooling of multiplexed sequencing samples, clustering and sequencing were carried out as recommended by the manufacturer on Illumina HiSeq 2500 or HiSeq 4000. For bisulfite-converted libraries, at least 50% of balanced libraries or Phix were multiplexed to overcome the imbalance of GC ratio. All libraries were sequenced in paired-end mode.

Analysis of methylation data

Raw reads were first trimmed as paired-end reads using Trimmomatic with default parameters to remove the adapters and low quality reads. Trimmed reads were aligned to mm9 using Bismark (v12.5). PCR duplications were removed with Picard (http://broadinstitute.github.io/picard/). CpG methylation level were calculated by Bis-SNP in bissnp_easy_usage.pl with default parameters.

Analysis of Hi-C data

All sequence data were produced using Illumina paired-end sequencing. Each end of the raw reads was mapped separately to the mm9 reference genome using BWA-mem. Filtered reads were then paired and de-duplicated (Picard). Reads that map to the same fragment were further removed. Contact matrices were generated at different resolution using Juicer pipeline with KR normalization and visualized using Juicebox. Loops were then called by HICCUPS.

Methyl-HiC reads mapping by Bhmem

Raw reads were first trimmed as paired-end reads using Trimmomatic with default parameters to remove the adapters and low-quality reads. All C in mm9 reference genome are converted to T to make C_to_T reference genome, and all G are converted to A to make G_to_A reference genome. On paired-end reads, C is converted to T in end 1 and G is converted to A in end 2. The converted end 1 and end 2 are joined as single paired fragment when both of them were mapped to C_to_T reference genome or G_to_A reference genome by BWA-MEM. Only unique mapped and passed VendorQualityFilter reads on both ends were joined. The best paired reads were selected based on the following priorities: (1) mapping quality on both ends are bigger than 0. (2) the sum of mapping quality score is larger. (3) both ends of reads are mapped into the same chromosome. (4) the sum of alignment score is larger. (5) the sum of mismatches is smaller. (6) the sum of matched cigar string length is larger. Only best paired reads were output for the following analysis. Low quality reads (not unique mapped on both ends, PCR duplicate and mapping quality score < 30) were removed for the following downstream analysis. Only bases with quality score more than 5 were included in the downstream methylation analysis. Details were implemented in Bhmem.java.

Methylation concordance analysis in Methyl-HiC

Bisulfite incompletely converted reads and 5' end incompletely converted cytosine (M-bias) were filtered out as that in Bis-SNP[38]. Only read pairs with methylation level at both ends were kept for the methylation concordance analysis. For the regions of interests, such as HiCCUPS loops anchor regions, Pearson correlation coefficient (PCC) was calculated by the methylation level at each end of paired reads rather than by the average methylation level at each end of paired regions. Only reads with at least 20kb distant from each end were considered for the long-range methylation concordance. Expected control was generated by shuffling the read pairs within the same genomic regions. Fisher z-transformation, implemented in function of "cocor.indep.groups" at R package "cocor" was used to determine the significance between observed PCC and control PCC. Details were implemented in MethyCorAcrossHiccups.java.

Single cell Methyl-HiC analysis

Reads were mapped by the same Bhmem pipeline with additional parameters to adapt the single cell protocol (-nonDirectional -pbat, G is converted to A in end 1 and C is converted to T in end 2; End 1 and end 2 mapped to different bisulfite converted genomes were also considered as the candidate of best pair when join them). We also utilize the restriction enzyme cutting sites on the reference genome to help the reads mapping. Only read pairs with restriction enzyme cutting sites nearby the reads (+/-50bp nearby alignment start and end of the reads) were kept for the further analysis.

After removing low quality reads (not unique mapped, PCR duplicate, not both ends unique mapped and mapping quality score < 30), cells with less than 250,000 reads and 10,000 ligation events were removed for the further analysis. Finally, there are 47 naïve cells and 103 primed cells left for all of the single cell analysis.

Methylation density (total_methylated_count/total_count) was calculated in each non-overlapped 1Mb window at mm9 autosome chromosomes. Missing data was replaced by the mean methylation level at the same bin across all single cells. Bins with missing data in all of cells were removed from analysis. Then t-Distributed Stochastic Neighbor Embedding (t-SNE) was applied to represent the methylation level structure in single cell level (Rtsne package in R 3.4.0 with plexity=10 and max_iter=5000). Different plexity level and random seed were applied to test the robustness of representation. Methylated count and total count (missing data is not replaced by mean value yet) at each window within each sub-cluster was aggregated and then calculated the methylation level. Methylation level at each CpG from external ENCODE methylomes were liftovered from mm10 to mm9. Overlapped CpGs after liftover were discarded. Methylation density was calculated in each non-overlapped 1Mb window for ENCODE data. Bins with missing data in all of samples were removed from analysis. Euclidean distance between 3 merged sub-clusters in single cell Methyl-HiC and external ENCODE methylomes was calculated and clustered by “ward.D2” by hclust function in R. BAM files were merged within each sub-cluster and then visualized for Hi-C contact frequency by Juicebox (1.9.0)

Replication timing

Wavelet-smoothed of mean late/early S-phase ratios data by Repli-ChIP is obtained from ENCODE in ES-46C cell line. Regions with high values indicate domains of early replication where initiation occurs earlier in S-phase or early in a higher proportion of cells.

Data availability

Figures show merged data from all replicates. The Methyl-HiC, single cell Methyl-HiC, and WGBS data sets generated in this study have been deposited in the Gene Expression Omnibus (GEO) under the accession number GSE119171. Previously published data used for this study are listed in Supplementary Table 4. All the source code for Methyl-HiC analysis is publicly available at Bitbucket: https://bitbucket.org/dnaase/bisulfitehic/src/master/

References

1. Iurlaro, M., von Meyenn, F. & Reik, W. DNA methylation homeostasis in human and mouse development. *Current Opinion in Genetics & Development* **43**, 101-109 (2017).
2. Guo, J.U., Su, Y., Zhong, C., Ming, G.-l. & Song, H. Hydroxylation of 5-methylcytosine by TET1 promotes active DNA demethylation in the adult brain. *Cell* **145**, 423-434 (2011).
3. Lyko, F. The DNA methyltransferase family: a versatile toolkit for epigenetic regulation. *Nat Rev Genet* **19**, 81-92 (2018).
4. Guo, S. *et al.* Identification of methylation haplotype blocks aids in deconvolution of heterogeneous tissue samples and tumor tissue-of-origin mapping from plasma DNA. *Nature Genetics* **49**, 635 (2017).
5. Shoemaker, R., Deng, J., Wang, W. & Zhang, K. Allele-specific methylation is prevalent and is contributed by CpG-SNPs in the human genome. *Genome Research* **20**, 883-889 (2010).
6. Lister, R. *et al.* Human DNA methylomes at base resolution show widespread epigenomic differences. *Nature* **462**, 315 (2009).
7. Flusberg, B.A. *et al.* Direct detection of DNA methylation during single-molecule, real-time sequencing. *Nature Methods* **7**, 461 (2010).

8. Rand, A.C. *et al.* Mapping DNA methylation with high-throughput nanopore sequencing. *Nature Methods* **14**, 411 (2017).
9. Dixon, Jesse R., Gorkin, David U. & Ren, B. Chromatin Domains: The Unit of Chromosome Organization. *Molecular Cell* **62**, 668-680 (2016).
10. Schmitt, A.D., Hu, M. & Ren, B. Genome-wide mapping and analysis of chromosome architecture. *Nature Reviews Molecular Cell Biology* **17**, 743 (2016).
11. Lieberman-Aiden, E. *et al.* Comprehensive Mapping of Long-Range Interactions Reveals Folding Principles of the Human Genome. *Science* **326**, 289 (2009).
12. Rao, Suhas S.P. *et al.* A 3D Map of the Human Genome at Kilobase Resolution Reveals Principles of Chromatin Looping. *Cell* **159**, 1665-1680 (2014).
13. Yang, T. *et al.* HiCRep: assessing the reproducibility of Hi-C data using a stratum- adjusted correlation coefficient. *Genome Research* (2017).
14. Fortin, J.-P. & Hansen, K.D. Reconstructing A/B compartments as revealed by Hi-C using long-range correlations in epigenetic data. *Genome Biology* **16**, 180 (2015).
15. Yue, F. *et al.* A comparative encyclopedia of DNA elements in the mouse genome. *Nature* **515**, 355 (2014).
16. Jones, P.A. Functions of DNA methylation: islands, start sites, gene bodies and beyond. *Nature Reviews Genetics* **13**, 484 (2012).
17. Luo, C. *et al.* Single-cell methylomes identify neuronal subtypes and regulatory elements in mammalian cortex. *Science* **357**, 600 (2017).
18. Smallwood, S.A. *et al.* Single-cell genome-wide bisulfite sequencing for assessing epigenetic heterogeneity. *Nature Methods* **11**, 817 (2014).
19. Guo, H. *et al.* Single-cell methylome landscapes of mouse embryonic stem cells and early embryos analyzed using reduced representation bisulfite sequencing. *Genome Research* **23**, 2126-2135 (2013).
20. Nagano, T. *et al.* Single-cell Hi-C reveals cell-to-cell variability in chromosome structure. *Nature* **502**, 59-64 (2013).
21. Stevens, T.J. *et al.* 3D structures of individual mammalian genomes studied by single-cell Hi-C. *Nature* **544**, 59 (2017).
22. Ramani, V. *et al.* Massively multiplex single-cell Hi-C. *Nat Methods* **14**, 263-266 (2017).
23. Nagano, T. *et al.* Cell-cycle dynamics of chromosomal organization at single-cell resolution. *Nature* **547**, 61-67 (2017).
24. Flyamer, I.M. *et al.* Single-nucleus Hi-C reveals unique chromatin reorganization at oocyte-to-zygote transition. *Nature* **544**, 110 (2017).
25. Brons, I.G.M. *et al.* Derivation of pluripotent epiblast stem cells from mammalian embryos. *Nature* **448**, 191 (2007).
26. Durand, N.C. *et al.* Juicebox Provides a Visualization System for Hi-C Contact Maps with Unlimited Zoom. *Cell systems* **3**, 99-101 (2016).

27. Rhind, N. & Gilbert, D.M. DNA Replication Timing. *Cold Spring Harbor perspectives in biology* **5**, a010132-a010132 (2013).
28. Pope, B.D. *et al.* Topologically associating domains are stable units of replication-timing regulation. *Nature* **515**, 402 (2014).
29. Suzuki, M. *et al.* Late-replicating heterochromatin is characterized by decreased cytosine methylation in the human genome. *Genome Research* **21**, 1833-1840 (2011).
30. Hiratani, I. *et al.* Global reorganization of replication domains during embryonic stem cell differentiation. *PLoS Biol* **6**, 0060245 (2008).
31. Gilbert, D.M. Replication timing and transcriptional control: beyond cause and effect. *Current Opinion in Cell Biology* **14**, 377-383 (2002).
32. Rivera-Mulia, J.C. *et al.* Allele-specific control of replication timing and genome organization during development. *Genome Research* **28**, 800-811 (2018).
33. Schwartzman, O. & Tanay, A. Single-cell epigenomics: techniques and emerging applications. *Nature Reviews Genetics* **16**, 716 (2015).
34. Rodríguez-Carballo, E. *et al.* The HoxD cluster is a dynamic and resilient TAD boundary controlling the segregation of antagonistic regulatory landscapes. *Genes & Development* **31**, 2264-2281 (2017).
35. Lupiáñez, Darío G. *et al.* Disruptions of Topological Chromatin Domains Cause Pathogenic Rewiring of Gene-Enhancer Interactions. *Cell* **161**, 1012-1025 (2015).
36. Liu, Y. *et al.* Bisulfite-free, Base-resolution, and Quantitative Sequencing of Cytosine Modifications. *bioRxiv* (2018).
37. Tan, L., Xing, D., Chang, C.-H., Li, H. & Xie, X.S. Three-dimensional genome structures of single diploid human cells. *Science* **361**, 924 (2018).
38. Liu, Y., Siegmund, K.D., Laird, P.W. & Berman, B.P. Bis-SNP: Combined DNA methylation and SNP calling for Bisulfite-seq data. *Genome Biology* **13**, R61 (2012).
39. Clark, S.J. *et al.* scNMT-seq enables joint profiling of chromatin accessibility DNA methylation and transcription in single cells. *Nature Communications* **9**, 781 (2018).
40. Cao, J. *et al.* Joint profiling of chromatin accessibility and gene expression in thousands of single cells. *Science* (2018).
41. Gribnau, J., Hochedlinger, K., Hata, K., Li, E. & Jaenisch, R. Asynchronous replication timing of imprinted loci is independent of DNA methylation, but consistent with differential subnuclear localization. *Genes Dev* **17**, 759-73 (2003).
42. Stadler, M.B. *et al.* DNA-binding factors shape the mouse methylome at distal regulatory regions. *Nature* **480**, 490 (2011).

Acknowledgments

We thank Samantha Kuan and Dr. Bin Li for processing of sequencing. We also thank Dr. Ramya Raviram for kindly revision and comments on the manuscript. Funding from the NIH 4D Nucleome program (U54DK107977) supported the project. G.L. and B.R. were supported by NIH 4D Nucleome program (U54DK107977). Y.L. and M.K. were supported by funding from NIH 1U01HG007610-01.

Author contributions

B.R., Y.L., and G.L. conceived the study and prepared the manuscript. G.L. performed the Methyl-HiC and single cell Methyl-HiC experiments. Y.L. wrote new Methyl-HiC analysis pipeline and performed the analysis. Y.L. and G.L. performed the *in situ* Hi-C and WGBS analysis. G.L. and Y.L. wrote the manuscripts with the guidance of M.K. and B.R. Correspondence and requests for materials should be addressed to B.R. (biren@ucsd.edu)

Competing financial interests

The authors declare no competing financial interests.

Figure Legends

Fig.1 Methyl-HiC simultaneously profiles long-range chromatin interactions and DNA methylome in mouse embryonic stem cells.

a) The workflow of Methyl-HiC. Biotin-enriched DNA fragments from *in situ* Hi-C are bisulfite converted followed by paired-end sequencing. The short sequencing reads are mapped to the genome and processed by the in-house computational pipeline Bhmem.
b) An illustration shows the methylation status on read pairs supporting a chromatin loop. Methylation status are determined by CpG sites on the reads.
c) Comparison of contact matrix between *in situ* Hi-C and Methyl-HiC at different resolutions. Blue squares are loops identified from corresponding dataset at 5kb resolution. Numbers below each map show the maximum values for the map color range.
d) Comparison of contact frequency distance decay curve obtained from *in situ* Hi-C and Methyl-HiC data.
e) Comparison of TADs identified from *in situ* Hi-C and Methyl-HiC.
f) Comparison of CpG sites covered by at least 10 reads in WGBS and Methyl-HiC.
g) DNA methylation levels for common CpGs are highly concordant between WGBS and Methyl-HiC.

Fig. 2 DNA methylation status is generally concordant between spatially proximal regions.

a) Pearson correlation coefficient of DNA methylation concordance between anchors of chromatin loops identified using HiCCUPS at 5kb and 25kb resolutions. Only reads containing 2 or more CpGs on each end were included. Paired reads located within the same loop anchors were re-shuffled and used to calculate the expected values.

b) Loops in compartment A show significantly higher concordance compared to those in compartment B.
c) Concordance of DNA methylation levels between regions bearing various chromatin states called by chromHMM. Pearson correlation coefficients of DNA methylation were calculated from reads that fall within any two chromatin states.

Fig.3 Simultaneous analysis of DNA methylome and chromatin architecture in individual cells by Single Cell Methyl-HiC

a) Workflow of Single cell Methyl-HiC.
b) Comparison of aggregate contact matrix from 103 primed mESCs single cell Methyl-HiC data and bulk Methyl-HiC. Contact matrixes were normalized by sequencing coverage.
c) Comparison of average global methylation level from single cell Methyl-HiC between primed and naïve mESCs.
d) DNA methylation concordance on loop anchors is validated in single cell Methyl-HiC datasets. Chromatin loops detected are from bulk Methyl-HiC by HiCCUPS.
e) Late replication regions defined by Repli-ChIP show significantly higher DNA methylation variation. SD means standard deviation.
f) Late replication regions defined by Repli-ChIP show significantly lower variation in chromatin contact. SD means standard diversion.

Fig.4 Single cell Methyl-HiC reveals heterogeneity of cultured mouse embryonic stem cells.

a) T-sne visualization of unsupervised clustering results according to DNA methylation. Methylation level is calculated in non-overlaping 1Mb bins.
b) Subgroups in primed cells show lineage specific DNA methylation. Cells from each cluster are aggregated and compared with tissue-specific methylome.
c) Pearson correlation matrixes of contact matrix from different cell clusters. The left map shows the bulk *in situ* Hi-C matrixes from primed and naïve cells,

respectively. Pearson correlation is calculated under 1Mb resolution. Color ranges have been set to the same scale.

d) GO biological process terms for DMRs in Compartment B in Cluster 2 while switch to Compartment A in Cluster 3.

e) GO biological process terms of genes switching from Compartment B in Cluster 2 to Compartment A in Cluster 3

f) Snapshot of *HoxD* cluster genes in different compartments between Cluster 2 and 3.

Fig.1

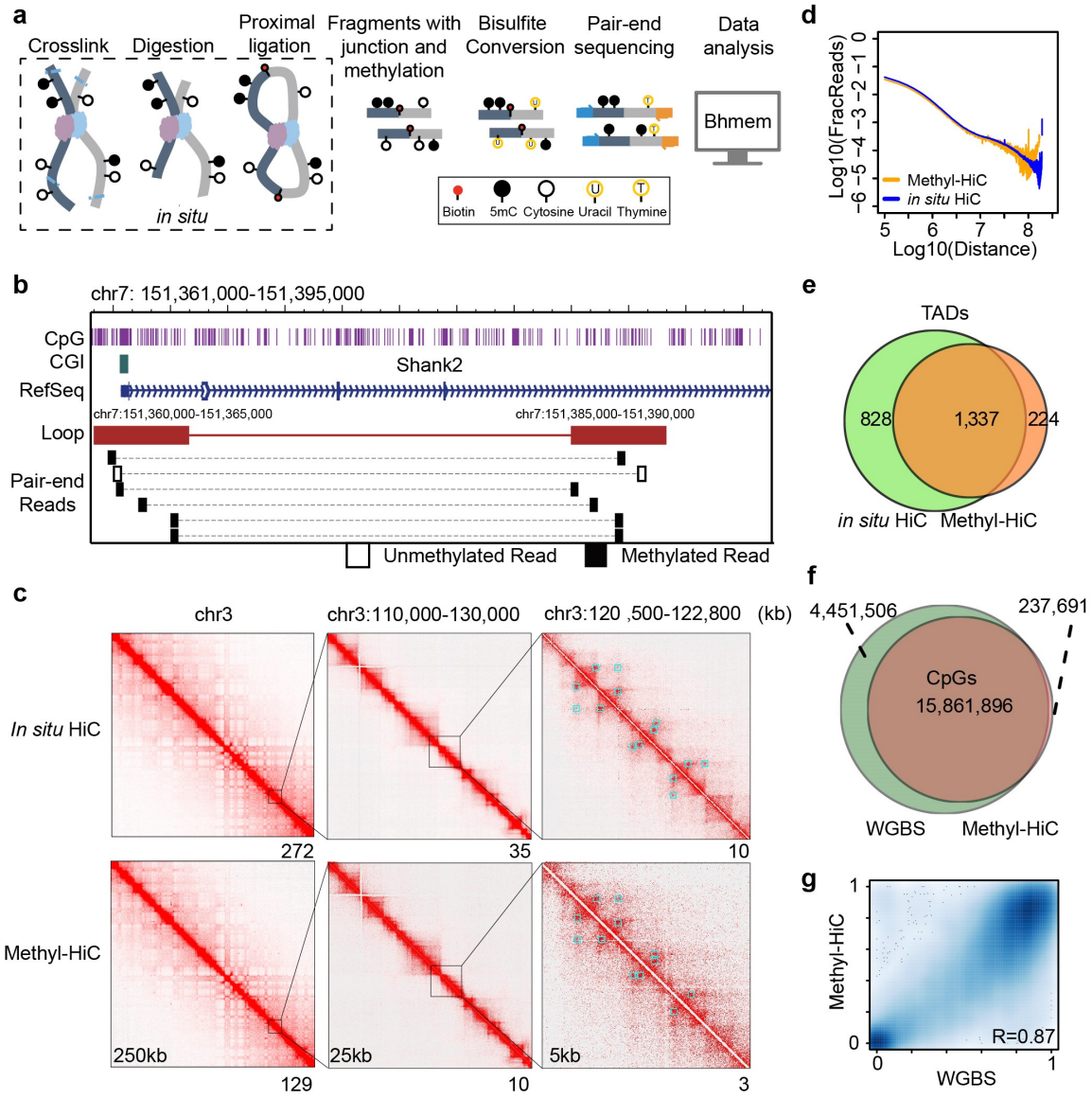

Fig.2

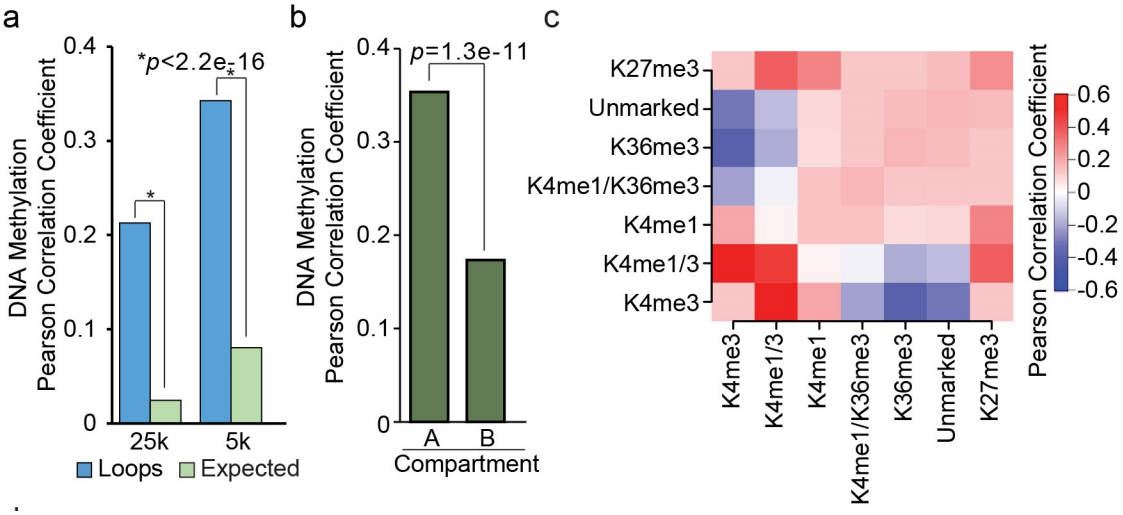

Fig.3

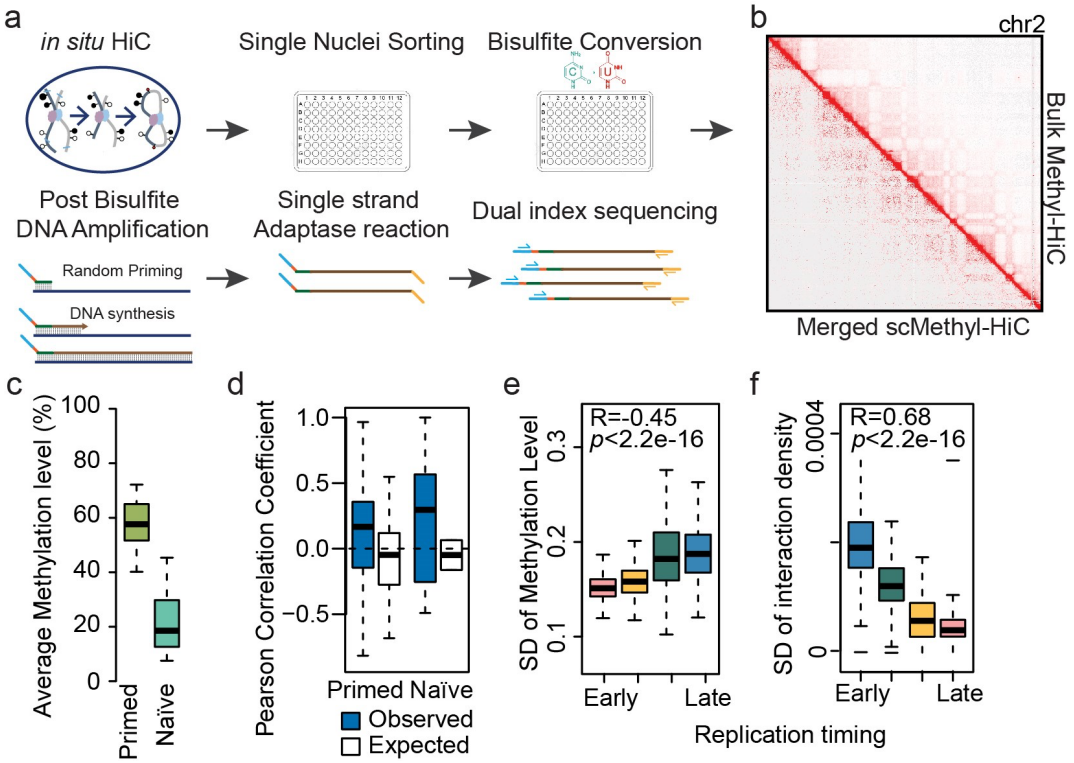

Fig.4

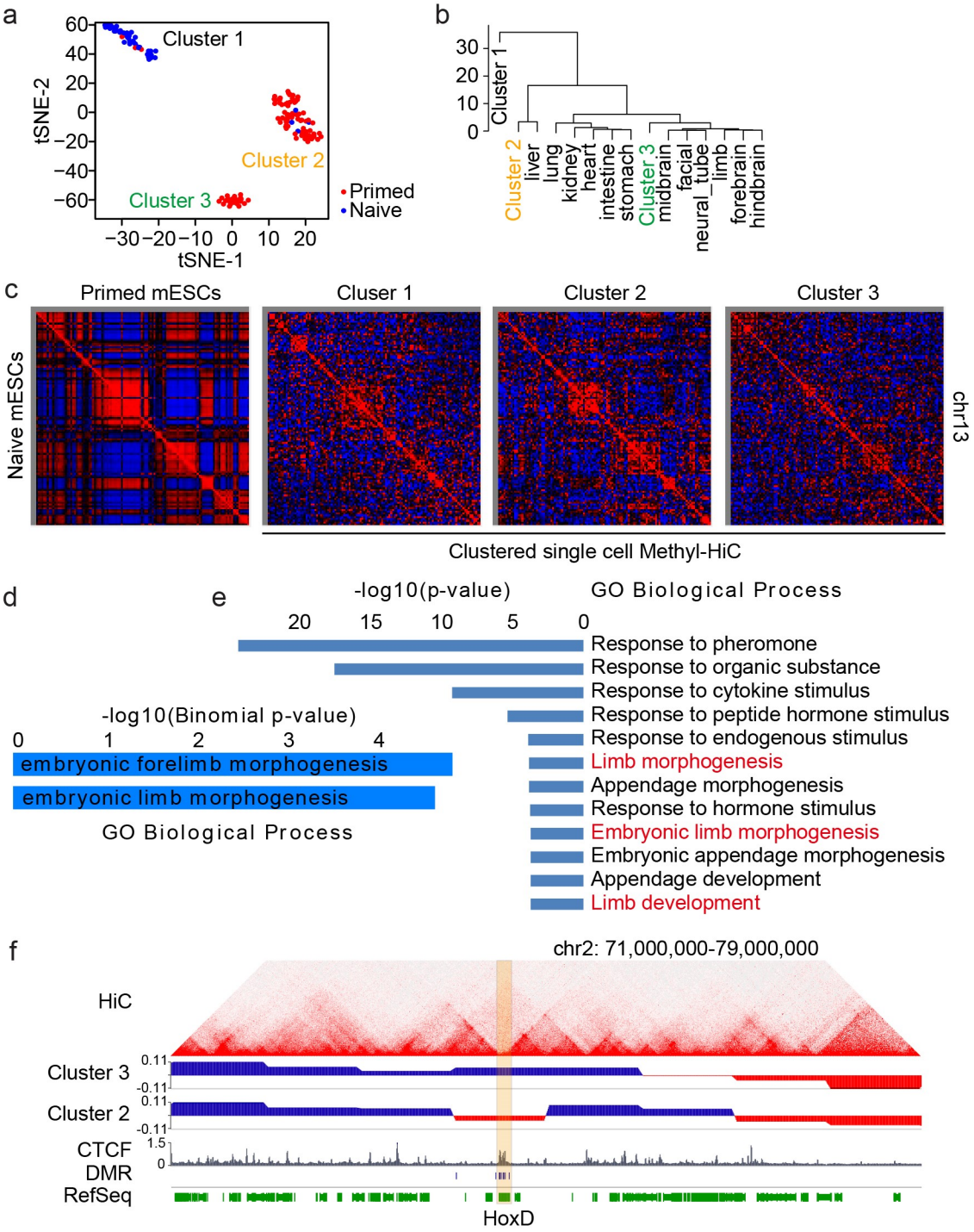

Supplementary Materials

Simultaneous profiling of DNA methylation and chromatin architecture in mixed populations and in single cells

Guoqiang Li[1,6], Yaping Liu[3,4,6], Yanxiao Zhang[1], Rongxin Fang[1,5], Manolis Kellis[3,4], Bing Ren[1,2]*

[1] Ludwig Institute for Cancer Research, La Jolla, CA 92093

[2] Department of Cellular and Molecular Medicine, Center for Epigenomics, Institute of Genomic Medicine, Moores Cancer Center, University of California, San Diego, School of Medicine, La Jolla, CA 92093

[3] Broad Institute of MIT and Harvard, Cambridge, MA 02142

[4] Massachusetts Institute of Technology, Computer Science and Artificial Intelligence Laboratory, Cambridge, MA 02139

[5] Bioinformatics and Systems Biology Graduate Program, University of California, San Diego, La Jolla, CA 92093

[6] Contributed equally

* email: biren@ucsd.edu

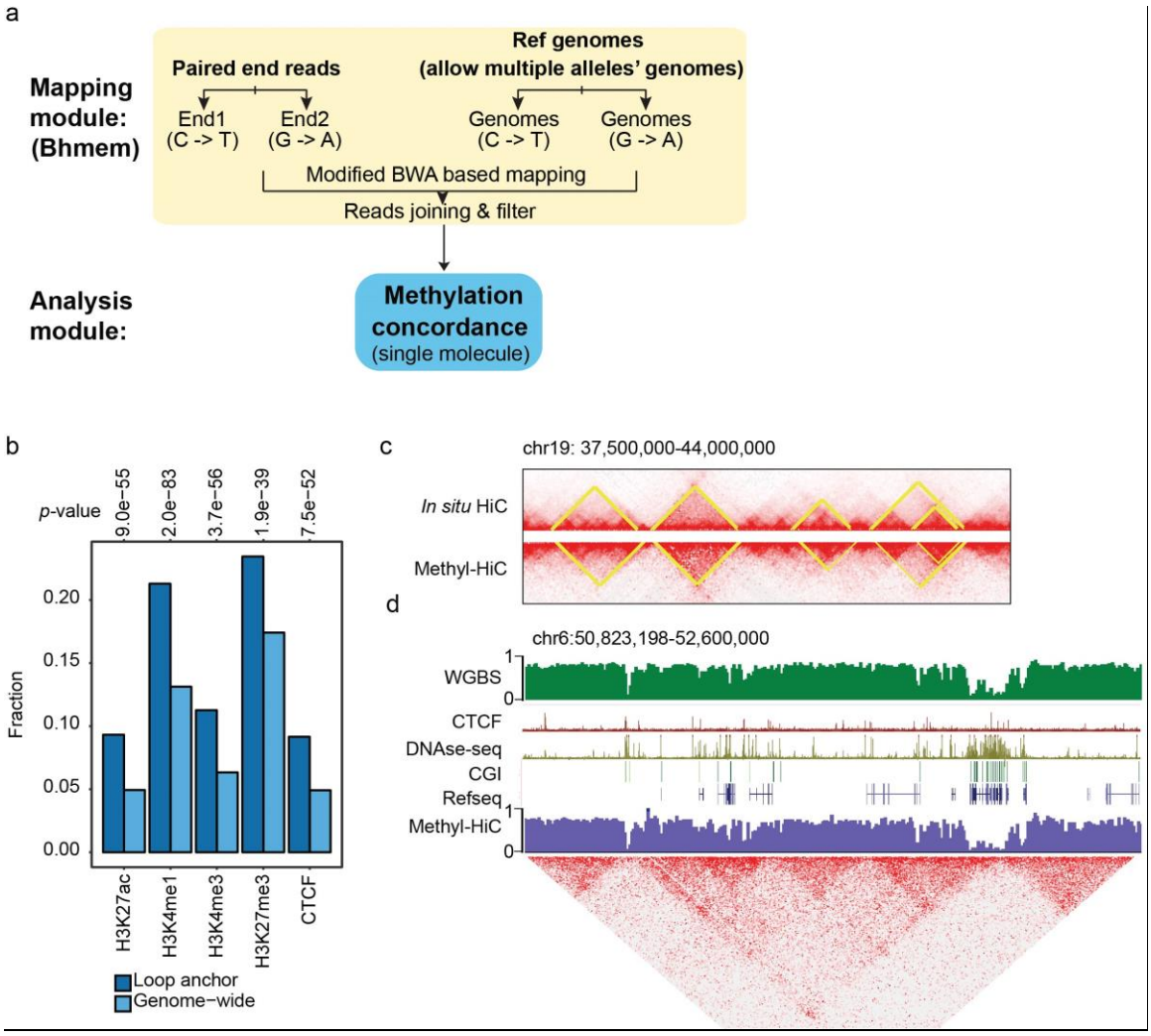

Fig. S1 Methyl-HiC simultaneously profiles long-range chromatin interactions and DNA methylome in mouse embryonic stem cells.

a. The Bhmem Methyl-HiC data mapping and analysis modules.

b. HiCCUPS loops called from Methyl-HiC dataset enrich enhancers and promoters with active histone markers, Polycomb-Repressed chromatin marked by H3k27me3, and CTCF.

c. Contact domains called from *in situ* HiC and Methyl-HiC, respectively

d. A snapshot of both DNA methylation and HiC contact matrix

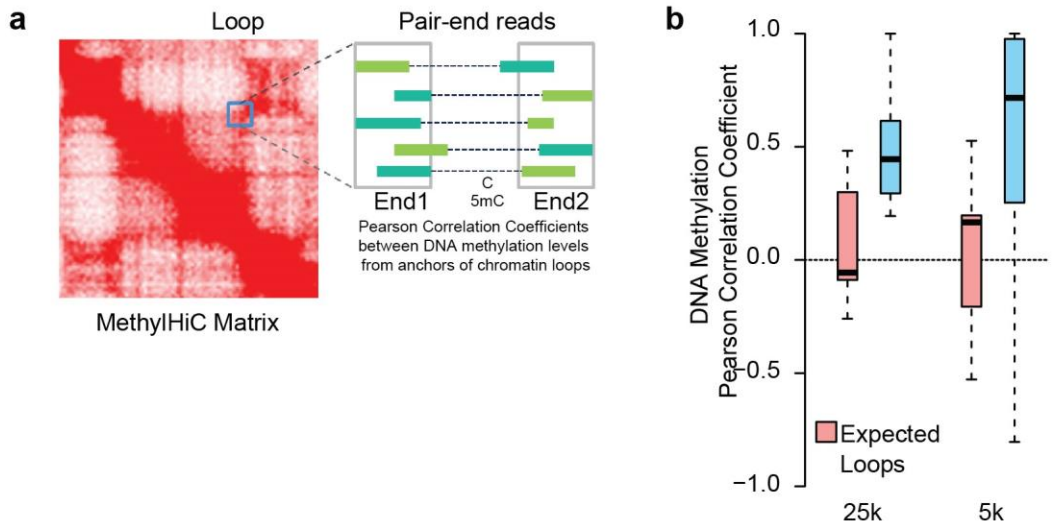

Fig. S2 DNA methylation status is generally concordant between spatially proximal regions.

a. Illustration of the calculation for methylation concordance on DNA loop anchors

b. Pearson correlation coefficients distribution of individual loops at two different resolutions.

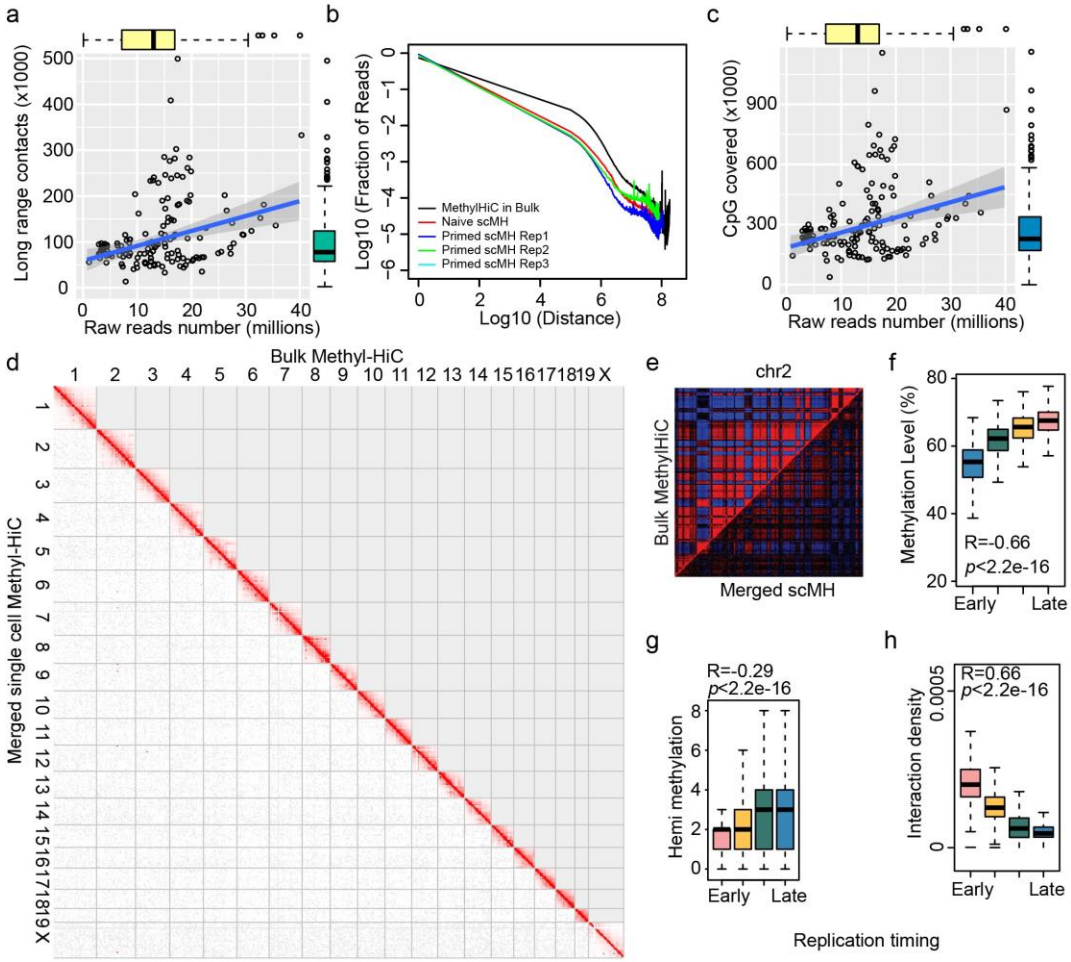

Fig.S3 Simultaneous analysis of DNA methylome and chromatin architecture in individual cells by Single Cell Methyl-HiC

a. The scatterplot for raw reads numbers and the number of CpG covered.

b. The scatterplot for raw reads numbers and the number of long range contacts.

c. Contact probability of merged single cell Methyl-HiC and bulk Methyl-HiC data.

d. Genome wide contact matrix comparison between resembled single cell Methyl-HiC data and bulk Methyl-HiC data.

e. Pearson correlation matrix comparison between ensemble single cell Methyl-HiC data and bulk Methyl-HiC data.

f. DNA methylation distribution in replication timing regions.

g. The hemimethylation density in replication timing regions.

h. Interaction density distribution in replication timing regions.

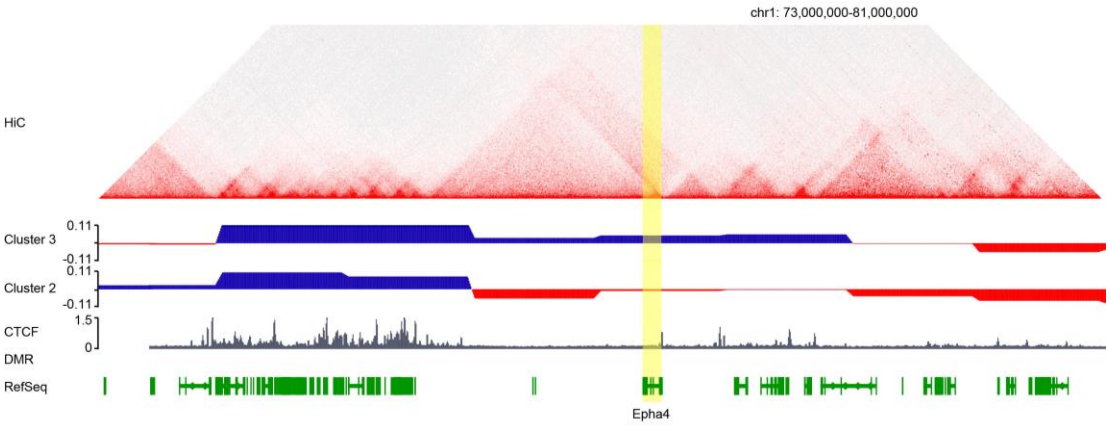

Fig.S4 Single cell Methyl-HiC reveals heterogeneity of cultured mouse embryonic stem cells.

The snapshot for *Epha4* gene in different compartments between Cluster 2 and Cluster 3.

Supplemental Table S2

Summary of single cell Methyl-HiC datasets

Cell_ID	Raw reads	Mapping rate	# Cpg	Methylation level	Contacts
JL_392_1.ACTTGA	26,093,135	29%	415192	51.5	156229
JL_392_1.CGATGT	30,625,688	29%	304672	52.0	111758
JL_392_1.GCCAAT	25,727,186	31%	481532	55.5	189239
JL_392_1.TAGCTT	32,943,089	32%	415179	57.8	168720
JL_392_10.ACTTGA	14,248,904	32%	441917	64.9	177312
JL_392_10.CGATGT	14,731,902	30%	618359	64.4	233451
JL_392_10.GCCAAT	14,602,294	33%	769826	44.5	273000
JL_392_10.TAGCTT	19,475,771	33%	698044	52.8	240987
JL_392_2.ACTTGA	9,203,085	45%	475615	55.9	191134
JL_392_2.CGATGT	9,866,361	41%	375493	49.6	149508
JL_392_2.TAGCTT	12,526,717	45%	563680	51.7	221783
JL_392_4.ACTTGA	14,421,839	31%	300475	63.9	122731
JL_392_4.CGATGT	18,785,018	31%	455483	51.1	177192
JL_392_4.GCCAAT	14,793,535	31%	406426	54.6	160037
JL_392_4.TAGCTT	18,823,301	36%	645062	44.8	249014
JL_392_5.ACTTGA	13,471,090	37%	546747	60.6	216535
JL_392_5.CGATGT	19,249,819	36%	662127	50.1	271298
JL_392_5.GCCAAT	12,694,096	37%	560169	45.7	228079
JL_392_5.TAGCTT	17,003,248	36%	407094	63.2	167700
JL_392_6.ACTTGA	15,189,668	37%	476449	54.1	183245
JL_392_6.CGATGT	22,250,955	34%	312421	60.3	118488
JL_392_6.GCCAAT	15,581,905	39%	666163	53.0	264422
JL_392_6.TAGCTT	17,957,120	39%	597161	65.3	229934
JL_392_7.ACTTGA	15,868,546	36%	620005	48.2	225881
JL_392_7.CGATGT	15,352,986	32%	375431	52.9	141105
JL_392_7.GCCAAT	12,010,704	37%	581526	51.3	221109
JL_392_7.TAGCTT	19,435,959	36%	514383	55.1	189150
JL_392_8.ACTTGA	15,729,248	66%	938407	52.6	396561
JL_392_8.CGATGT	16,756,268	64%	642571	63.0	289973
JL_392_8.GCCAAT	17,057,513	66%	1128721	50.9	486775
JL_392_8.TAGCTT	737,634	69%	114117	42.5	43026
JL_392_9.ACTTGA	16,506,754	36%	718715	45.3	269981
JL_392_9.CGATGT	19,148,429	31%	416172	61.6	175583
JL_392_9.GCCAAT	16,980,404	35%	609920	63.1	232840
JL_392_9.TAGCTT	39,848,719	35%	843267	61.7	319863
JL_443.ACTTGA	14,657,939	33%	276547	52.6	102898

JL_443.CGATGT	14,669,364	32%	232953	58.8	84373
JL_443.GCCAAT	18,913,126	32%	301762	56.6	94836
JL_443.TAGCTT	12,313,409	34%	220817	48.1	88043
JL_444.ACTTGA	15,812,080	52%	375132	50.1	136720
JL_444.CGATGT	16,281,750	52%	348045	44.3	133998
JL_444.GCCAAT	32,295,147	51%	375328	52.4	139611
JL_444.TAGCTT	12,572,838	47%	222240	59.7	81726
JL_445.ACTTGA	27,063,013	31%	356552	52.7	129134
JL_445.CGATGT	21,127,143	30%	266303	59.5	95930
JL_445.GCCAAT	43,200,603	29%	261127	64.3	99958
JL_445.TAGCTT	15,678,272	33%	252447	57.4	93608
JL_446.ACTTGA	14,036,738	32%	287828	60.2	105693
JL_446.CGATGT	13,073,876	31%	231288	58.7	83761
JL_446.GCCAAT	28,983,280	30%	299361	55.8	104180
JL_446.TAGCTT	11,148,380	34%	285567	58.6	105016
JL_447.ACTTGA	17,297,213	38%	465375	57.3	170315
JL_447.CGATGT	16,588,103	37%	266615	56.5	103432
JL_447.GCCAAT	35,112,622	36%	329496	53.2	123091
JL_447.TAGCTT	15,207,963	38%	339200	60.0	130483
JL_458_10.ACTTGA	10,125,956	25%	185497	69.3	61389
JL_458_10.CGATGT	9,541,620	24%	93071	71.9	31811
JL_458_10.GCCAAT	19,808,580	24%	135512	71.4	46913
JL_458_10.TAGCTT	6,944,940	26%	91324	64.1	33960
JL_458_11.ACTTGA	11,079,304	23%	118730	68.4	39662
JL_458_11.CGATGT	10,996,456	23%	132024	53.6	43607
JL_458_11.GCCAAT	26,677,844	23%	225236	42.3	74556
JL_458_11.TAGCTT	9,694,924	24%	169579	70.1	53096
JL_458_12.ACTTGA	12,507,624	24%	197443	57.5	66739
JL_458_12.CGATGT	12,769,904	24%	108458	66.1	35355
JL_458_12.GCCAAT	18,892,680	24%	139780	65.3	45821
JL_458_12.TAGCTT	8,911,728	26%	104243	68.2	28529
JL_458_1.ACTTGA	12,151,968	24%	130488	61.5	45549
JL_458_1.CGATGT	18,534,848	25%	110278	63.1	36772
JL_458_1.GCCAAT	17,254,304	24%	165175	22.5	59649
JL_458_1.TAGCTT	16,010,560	24%	150292	70.1	43914
JL_458_2.ACTTGA	11,928,260	22%	112884	73.6	34961
JL_458_2.CGATGT	19,987,384	23%	146790	48.1	49958
JL_458_2.GCCAAT	17,053,004	22%	135658	72.3	49325
JL_458_2.TAGCTT	13,411,156	23%	108664	57.7	38972
JL_458_3.ACTTGA	15,112,552	24%	186980	70.1	52288
JL_458_3.CGATGT	21,907,036	24%	149058	59.3	54085

JL_458_3.GCCAAT	12,796,920	24%	109756	74.1	39170
JL_458_3.TAGCTT	17,488,800	23%	100136	58.3	34347
JL_458_4.ACTTGA	17,057,300	22%	181459	74.1	67891
JL_458_4.CGATGT	26,805,892	22%	195090	39.0	61936
JL_458_4.GCCAAT	20,922,184	22%	149753	69.5	51931
JL_458_4.TAGCTT	20,544,428	21%	143436	73.4	53652
JL_458_5.ACTTGA	15,258,496	24%	207326	16.9	60300
JL_458_5.CGATGT	25,030,480	24%	202581	36.3	66115
JL_458_5.GCCAAT	21,508,396	23%	197997	70.7	54536
JL_458_5.TAGCTT	18,179,820	23%	110883	46.8	31124
JL_458_6.ACTTGA	12,136,332	22%	161285	44.7	52259
JL_458_6.CGATGT	21,484,344	23%	116883	69.2	22697
JL_458_6.GCCAAT	18,010,880	22%	149513	57.2	51895
JL_458_6.TAGCTT	14,255,808	22%	94886	71.7	33498
JL_458_7.ACTTGA	14,654,416	26%	236029	54.4	84571
JL_458_7.CGATGT	15,929,132	26%	181125	70.8	62794
JL_458_7.GCCAAT	29,142,676	26%	309934	44.9	102963
JL_458_7.TAGCTT	11,541,720	27%	240599	69.7	84816
JL_458_8.ACTTGA	11,567,744	23%	199435	51.9	73004
JL_458_8.CGATGT	11,000,676	23%	140007	71.9	41557
JL_458_8.GCCAAT	27,394,804	22%	269659	68.7	84724
JL_458_8.TAGCTT	10,943,320	24%	170781	35.8	61502
JL_458_9.ACTTGA	12,064,072	24%	186427	66.8	61696
JL_458_9.CGATGT	14,643,372	24%	98179	63.5	20855
JL_458_9.GCCAAT	24,487,096	23%	173215	73.4	62719
JL_458_9.TAGCTT	9,426,776	25%	184927	71.1	39774
Naïve state mESCs					
JL_457_1.ACTTGA	2,536,610	39%	238554	36.00	82225
JL_457_1.CGATGT	3,519,177	34%	181273	20.72	63011
JL_457_1.GCCAAT	2,954,766	40%	250614	20.88	84559
JL_457_1.TAGCTT	3,347,255	40%	211478	47.65	67756
JL_457_10.ACTTGA	5,876,679	39%	249658	15.92	84532
JL_457_10.CGATGT	6,008,416	38%	252337	41.13	78883
JL_457_10.GCCAAT	12,932,458	36%	238947	49.93	77548
JL_457_10.TAGCTT	8,038,440	38%	211939	9.41	71326
JL_457_11.ACTTGA	6,846,864	41%	211261	15.06	68826
JL_457_11.CGATGT	6,998,509	41%	206123	31.13	67457
JL_457_11.GCCAAT	14,773,266	38%	231155	24.67	76463
JL_457_11.TAGCTT	8,287,532	39%	208065	25.38	63253
JL_457_12.ACTTGA	6,396,872	39%	176531	19.11	58221
JL_457_12.CGATGT	6,707,715	38%	122955	36.36	38579

JL_457_12.GCCAAT	12,866,407	37%	239563	23.88	76129
JL_457_12.TAGCTT	7,050,902	39%	177155	18.03	55256
JL_457_2.ACTTGA	3,297,537	40%	236253	54.48	78462
JL_457_2.CGATGT	4,880,589	35%	170253	13.33	56416
JL_457_2.GCCAAT	4,056,438	37%	202682	26.20	67272
JL_457_2.TAGCTT	3,058,499	41%	239417	9.52	76676
JL_457_3.ACTTGA	2,864,751	38%	204671	7.16	69760
JL_457_3.CGATGT	4,249,908	34%	198578	30.51	61411
JL_457_3.GCCAAT	3,603,828	37%	272433	7.34	83459
JL_457_3.TAGCTT	2,532,295	40%	206214	14.21	62123
JL_457_4.ACTTGA	2,898,234	51%	192612	12.36	62311
JL_457_4.CGATGT	4,402,393	49%	213442	33.97	60602
JL_457_4.GCCAAT	4,005,945	49%	249647	12.21	76826
JL_457_4.TAGCTT	3,875,006	44%	173367	16.78	57325
JL_457_5.ACTTGA	3,103,932	37%	210337	32.97	71349
JL_457_5.CGATGT	4,625,915	33%	193543	11.42	60829
JL_457_5.GCCAAT	3,983,288	36%	237047	17.72	81594
JL_457_5.TAGCTT	3,037,584	39%	198308	14.26	70924
JL_457_6.ACTTGA	2,598,758	36%	180467	9.96	60204
JL_457_6.CGATGT	3,900,947	33%	146873	21.32	42386
JL_457_6.GCCAAT	3,571,898	36%	234174	17.93	73200
JL_457_6.TAGCTT	2,683,157	38%	179577	14.99	51550
JL_457_7.ACTTGA	8,108,550	41%	269301	12.73	85553
JL_457_7.CGATGT	7,374,836	40%	207175	9.04	61353
JL_457_7.GCCAAT	16,327,502	40%	309737	31.66	98812
JL_457_7.TAGCTT	8,162,721	42%	317509	29.47	93198
JL_457_8.ACTTGA	7,410,698	38%	345004	6.68	102615
JL_457_8.CGATGT	8,131,562	36%	175477	12.69	57794
JL_457_8.GCCAAT	13,393,982	35%	265145	9.36	82751
JL_457_8.TAGCTT	6,683,450	39%	247978	30.93	78801
JL_457_9.ACTTGA	8,309,914	40%	284553	20.75	93001
JL_457_9.CGATGT	7,686,532	40%	309111	23.46	90810
JL_457_9.GCCAAT	16,361,850	38%	340304	7.92	101201

Supplemental Table S3

Differential Compartments between Cluster 2 and 3 in single cell Methyl-HiC

Supplemental Table S4

Published data sets used in this study	Data Source	Reference
F123 *in situ* HiC	GSE86150	[1]
sNMseq	GSE97179	[2]
Chromatin states in mESCs	ENCODE	[3]
Single cell Methylome in primary and naïve mESCs	GSE56879	[4]

REFERENCES

1. Fang, R. *et al.* Mapping of long-range chromatin interactions by proximity ligation-assisted ChIP-seq. *Cell Research* **26**, 1345 (2016).
2. Luo, C. *et al.* Single-cell methylomes identify neuronal subtypes and regulatory elements in mammalian cortex. *Science* **357**, 600 (2017).
3. Yue, F. *et al.* A comparative encyclopedia of DNA elements in the mouse genome. *Nature* **515**, 355 (2014).
4. Smallwood, S.A. *et al.* Single-cell genome-wide bisulfite sequencing for assessing epigenetic heterogeneity. *Nature Methods* **11**, 817 (2014).